Fundamentals and Applications of Mo and Nb Alloying in High Performance Steels – Volume 2
Edited by Hardy Mohrbacher
CBMM, IMOA and TMS, 2015

EFFECTS OF COMBINING NIOBIUM AND MOLYBDENUM IN HSLA STEELS: FROM AUSTENITE CONDITIONING TO FINAL MICROSTRUCTURE

N. Isasti, B. Pereda, B. López, J.M. Rodriguez-Ibabe and P. Uranga

CEIT and TECNUN (University of Navarra), Donostia-San Sebastian, Basque Country, Spain

Keywords: Austenite Conditioning, Phase Transformations, EBSD Quantification, Microstructure, Mechanical Properties

Abstract

Three main topics are covered in this paper regarding Nb-Mo interactions in microalloyed steels. First, the synergistic behavior of Nb and Mo in enhancing solute drag effects and modifying recrystallization and precipitation kinetics in austenite under hot working conditions is analyzed. Then, the effect of different microalloying additions on the final phase transformations is examined. In addition to composition and austenite conditioning effects on the phases formed and the corresponding CCT diagrams, a quantitative study using an EBSD technique is described which was performed in order to measure unit size distributions and homogeneity of complex microstructures. Finally, the contribution of different strengthening mechanisms to yield strength is evaluated for different coiling temperatures and compositions.

Introduction

Nowadays, combinations of high strength and high toughness are required for applications such as gas and oil transportation pipes, offshore facilities and naval technologies [1,2]. Suitable combinations of microalloying additions contribute to an increase in strength directly through microstructural refinement, solid solution strengthening and precipitation hardening, as well as indirectly, through enhanced hardenability and associated modification of the resultant microstructure [3]. Nevertheless, toughness may be impaired depending on the selected processing strategy followed to achieve the strength requirements.

In this context, Mo addition is a common practice to increase strength and toughness in low C steels because of its effect in promoting low temperature transformation products after hot rolling [4]. On the other hand, the use of Nb is well known because of its ability to retard recrystallization both by solute drag and by strain induced precipitation, which leads to pancaked austenite and, after transformation, provides fine room temperature microstructures with improved mechanical properties [5].

Obviously, this simplified approach needs to be modulated depending on the specific compositions of each steel grade and thermomechanical route because interactions between microalloying elements become complex and multiple effects are interacting at the same time. This paper seeks to analyze the different interactions during austenite conditioning and phase transformations. Resulting from the two previous steps, the mechanical strength will be modified and the balance of the different strengthening contributions will depend on the Nb and Mo effects on grain size refinement, dislocation substructure, second phase formation and precipitation.

Materials and Experimental

In the present study seven steels were studied, with two Nb levels (0.03 and 0.06%) and three Mo levels (0, 0.16 and 0.31%). A CMn steel was also used for comparison purposes only. All the steels were experimental heats and their chemical compositions are listed in Table I.

Table I. Chemical Compositions of the Steels (wt.%)

Steel	C	Mn	Si	Nb	Mo	Al	N
CMn	0.05	1.58	0.05	-	0.01	0.03	0.005
3NbMo0	0.05	1.6	0.06	0.029	0.01	0.028	0.005
3NbMo16	0.05	1.58	0.04	0.028	0.16	0.027	0.005
3NbMo31	0.05	1.57	0.05	0.028	0.31	0.028	0.005
6NbMo0	0.05	1.56	0.05	0.06	0.01	0.028	0.004
6NbMo16	0.05	1.6	0.05	0.061	0.16	0.03	0.005
6NbMo31	0.05	1.57	0.05	0.059	0.31	0.031	0.005

For the austenite conditioning, softening and strain induced precipitation kinetics determination, torsion samples with a gauge length of 17 mm and a diameter of 7.5 mm were machined from 40 mm thickness plates. The torsion tests were carried out using a computer controlled torsion machine. After reheating, the samples were deformed using pass strains ranging from 0.2 to 0.4 and different interpass times. The non-recrystallization temperature was determined by using the standard method proposed by Bai et al. [6].

For the phase transformation analysis, dilatometry tests were performed in a Bähr DIL805A/D quenching and deformation dilatometer. Solid cylinders with a diameter of 5 mm and a length of 10 mm were employed. The steels were subjected to different thermomechanical schedules in order to obtain different austenite conditions: undeformed, Cycle A, and deformed, Cycles B and C, respectively. A more detailed description of the procedure followed may be found in Reference 7. For the mechanical property evaluation, plane strain compression tests were performed. After deformation, the samples were cooled down at approximately 10 ºC/s to different coiling temperatures from 450 ºC to 650 ºC, so as to evaluate the effect of the coiling temperature on the phase transformation. Coiling was simulated by holding for 1 hour followed by slow cooling in the furnace to room temperature (≈1 ºC/s). The schemes of the different schedules are illustrated in Figures 1 and 2.

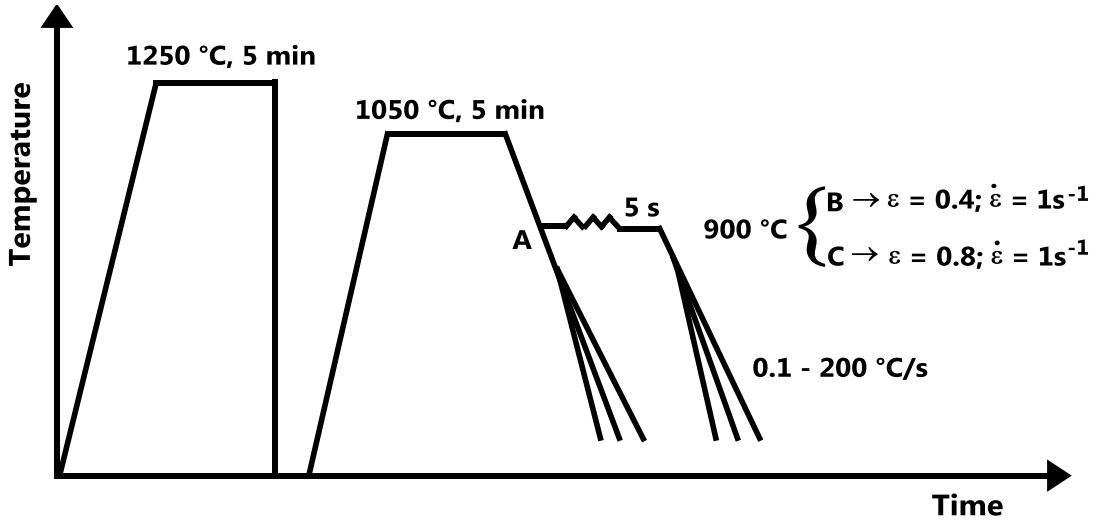

Figure 1. Schematic thermomechanical schedules applied for phase transformation analysis in dilatometry tests.

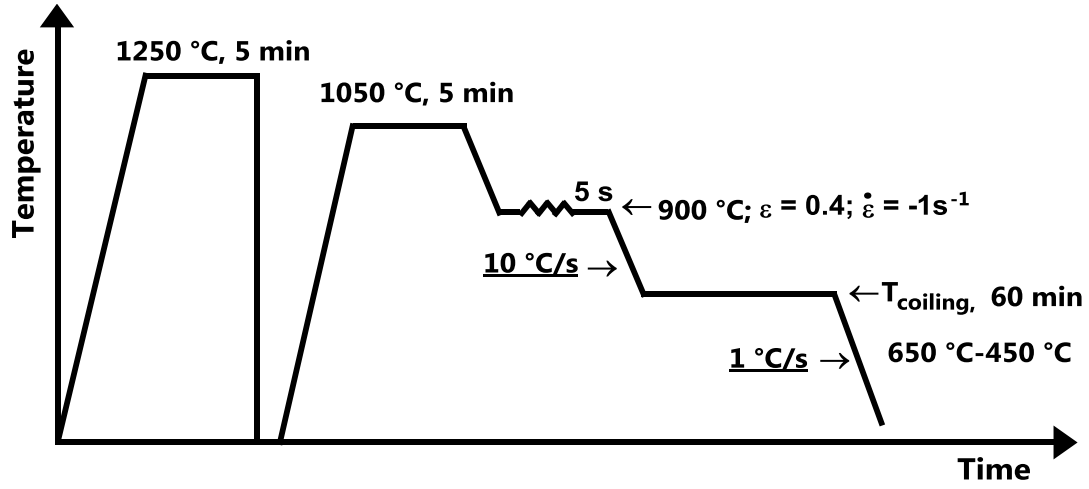

Figure 2. Schematic thermomechanical schedules for plane strain compression tests with different coiling temperatures (450, 550 and 650 ºC).

The microstructures obtained from the samples were characterized, after etching in 2% Nital, by different characterization techniques: Optical Microscopy, Scanning Electron Microscopy (SEM) and Field Emission Gun Scanning Electron Microscopy (FEGSEM). In addition to the optical and scanning electron microscopy analysis, a more detailed microstructural characterization was performed on selected specimens using the EBSD technique (Electron Back Scattered Diffraction). On these samples the ferrite unit sizes and the Kernel Average Misorientation (KAM) parameter were measured. Scan step sizes ranging from 0.2 μm, for high resolution scans, to 1 μm, for general microstructural characterization, were used. Tensile specimens were machined from the plane strain compression samples. Tensile specimens with a diameter of

4 mm and an initial length of 17 mm were tested. The tensile tests were performed at room temperature at a strain rate of 10^{-3} s^{-1}.

Austenite Conditioning

The strain accumulation within recrystallized austenite prior to transformation is one of the key factors in order to achieve a fine and homogeneous final microstructure. Nb and Mo, by means of solute drag and strain induced precipitation mechanisms, are the most efficient elements to retain strain during the final deformation passes. Therefore, a deep understanding of the softening mechanism and strain induced precipitation kinetics is needed. The semi-empirical equations to model these mechanisms have been evolving to adapt them to new grades and new technologies, such as the direct rolling of thin slabs. In this regard, the kinetics of static recrystallization of microalloyed steels, covering a wide austenite size range, were investigated in previous works [8]. Taking into account the effect of microalloying elements in solution, the deformation parameters (ε strain, $\dot{\varepsilon}$ strain rate and T absolute temperature) and the initial austenite grain size (D_o), the following equation was deduced for low carbon microalloyed steels:

$$t_{0.5} = 9.92x10^{-11} \cdot D_0 \cdot \varepsilon^{-5.6D_0^{-0.15}} \cdot \dot{\varepsilon}^{-0.53} \cdot \exp\left(\frac{180000}{RT}\right) \cdot \exp\left[\left(\frac{275000}{T} - 185\right) \cdot [Nb]_{eff}\right] \quad (1)$$

where $t_{0.5}$ is the time required for 50% recrystallization and $[Nb]_{eff}$ is the amount of Nb in solution.

Softening Kinetics for Nb-Mo Steels

The extension of Equation 1 to Nb-Mo steels required the evaluation of the Mo solute drag effect. Akben et al. [9], defined a Solute Retardation Parameter (SRP) for static recrystallization describing the retardation produced by additions of 0.1 wt.% of the different microalloyed elements. For Nb in Nb-Mo steels this parameter reached a value of SRP = 265, 1.19 times higher than the value obtained for Nb steels, SRP = 222. On the other hand, the value associated with Mo in Nb-Mo steels, SRP = 20 was 0.09 times lower than the SRP corresponding to Nb. Using this relationship, one can amend the definition of $[Nb]_{eff}$ such as to obtain the same drag effect as that produced by Nb in Nb-Mo steels; a 1.19xNb factor must be considered, and 0.09xMo (eg. to obtain the same drag effect as that produced by 1 wt.% Mo, an amount of 0.09 wt.% of Nb would be sufficient). These values are in good agreement with the experimental data obtained in this work for the lowest Nb content steels (0.03%Nb), whereas, in the case of 6NbMo16 and 6NbMo31 steels, these values tend to overestimate the experimental data. In this case, a value of 0.032 was obtained, which is three times lower than the value proposed for 0.03%Nb steels. This suggests a weaker effect of Mo in the presence of high Nb additions. Therefore, the resulting values for $[Nb]_{eff}$ in Equation 1 are:

$[Nb]_{eff} = [Nb]$ for Nb microalloyed steels;
$[Nb]_{eff} = 1.19[Nb] + 0.09[Mo]$ for 0.03%Nb-Mo microalloyed steels;
$[Nb]_{eff} = 1.19[Nb] + 0.032[Mo]$ for 0.06%Nb-Mo microalloyed steels.

The effect of Nb and Mo on the austenite evolution during multipass deformation can be complex and it depends both on the Nb and Mo contents and also on the deformation parameters. The softening and hardening mechanisms, including solute drag and strain-induced precipitation and the interactions between them, which can be different depending on the situation, are time and money consuming to evaluate only with experimental data. In this situation, the application of models coupling all the aforementioned factors can be a helpful tool in order to understand the interaction between softening and hardening mechanisms. In previous work, models describing the austenite microstructural evolution of Nb microalloyed steels during hot working were detailed [10,11]. These models were implemented with expressions adjusted for Nb-Mo, such as Equation 1. Combining multipass torsion tests and the model, some conclusions regarding strain accumulation before transformation can be drawn.

Non-recrystallization Temperature

Figure 3 shows, as an example, the mean flow stress curves obtained for four of the steels analyzed tested at $\varepsilon = 0.4$ and interpass time $t_{ip} = 30$ s. As can be observed, the increase in Nb content and the addition of Mo lead to higher T_{nr} values. For these specific conditions, the addition of 0.31%Mo increases the T_{nr} temperature from 970 to 1010 ºC in the case of 0.03%Nb and from 1030 to 1045 ºC for 0.06%Nb. This indicates a smaller influence of Mo for the higher Nb content in good agreement with the above mentioned weaker drag effect on recrystallization kinetics.

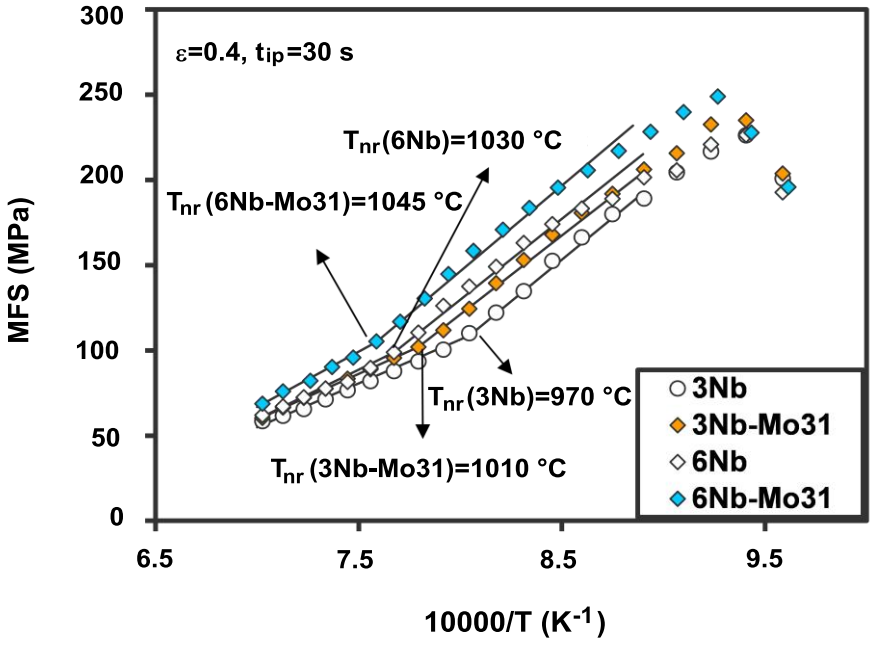

Figure 3. Mean flow stress against the inverse absolute temperature for steels 3NbMo0, 3NbMo31, 6NbMo0 and 6NbMo31.

In addition to composition, the non-recrystallization temperature depends also on deformation parameters, mainly pass strain and interpass time. The influence of interpass time is shown in Figure 4 for the condition corresponding to $\varepsilon = 0.4$. Firstly, for the lowest Nb content, 0.03%, there is a significant effect of Mo addition under all the test conditions considered. In contrast, when the Nb content increased to 0.06%, the addition of Mo seems to have less or even no influence. In the majority of the tests there were no differences in the T_{nr} values between the 6Nb, 6NbMo16 and 6NbMo31 steels. Only in the case of $t_{ip} = 30$ s and $\varepsilon = 0.4$ was there a small decrease in this temperature, for the 6Nb steel, not shown by the Mo-Nb grades. On the other hand, the increase in Mo content from 0.16 to 0.31% did not produce any change in the values of T_{nr} and was not dependent on the interpass time or pass strain.

Figure 5 shows the evolution of the measured and predicted softening fraction in both 3NbMo0 and 3NbMo31 steels for interpass times of 10 s and 30 s, Figure 5(a) and (b), respectively. It should be noted that in these calculations only recrystallization was taken into account, thus any deviation from the model can be interpreted as a result of the interaction with strain induced precipitation phenomena. As the temperature decreases the additional solute drag effect of Mo on the Nb-Mo steel plays an important role. The amount of softening starts to decrease at higher temperatures in this steel compared to the Nb steel, giving rise to higher values for T_{nr}. In the Nb steel, although initially the amount of softening dropped due to the solute drag of Nb, the T_{nr} is related to the interaction with precipitation, as is indicated by the deviation of the experimental results from the model below this temperature. Presumably, precipitation also takes place below this temperature in the Nb-Mo steel, since lower softening levels than predicted are measured in this range (after the ninth pass given at 986 ºC). This occurred well below the T_{nr} determined for this steel, denoting that in this case the additional drag effect of Mo was the controlling mechanism in retarding recrystallization, T_{nr} being related to it. Similar behavior is observed for 30 s, although in this case the longer interpass time available allowed more recrystallization to occur and the T_{nr} in both steels was somewhat lower.

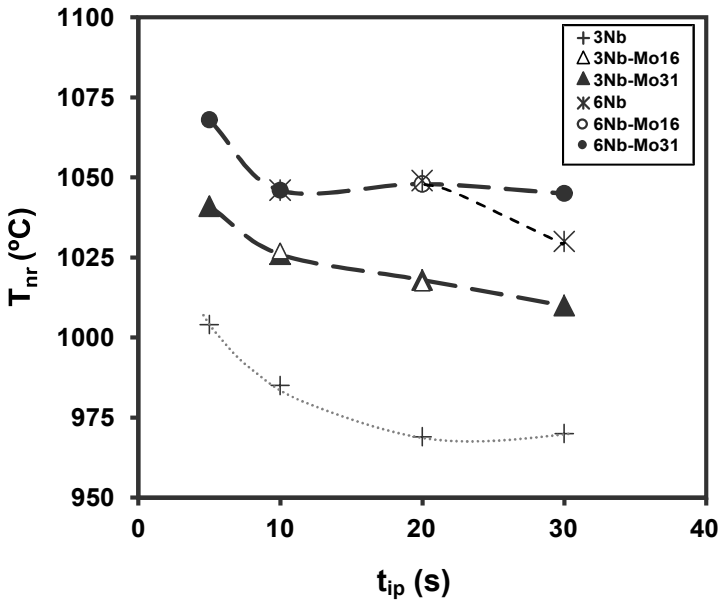

Figure 4. Dependence of T_{nr} on interpass time for a pass strain of $\varepsilon = 0.4$.

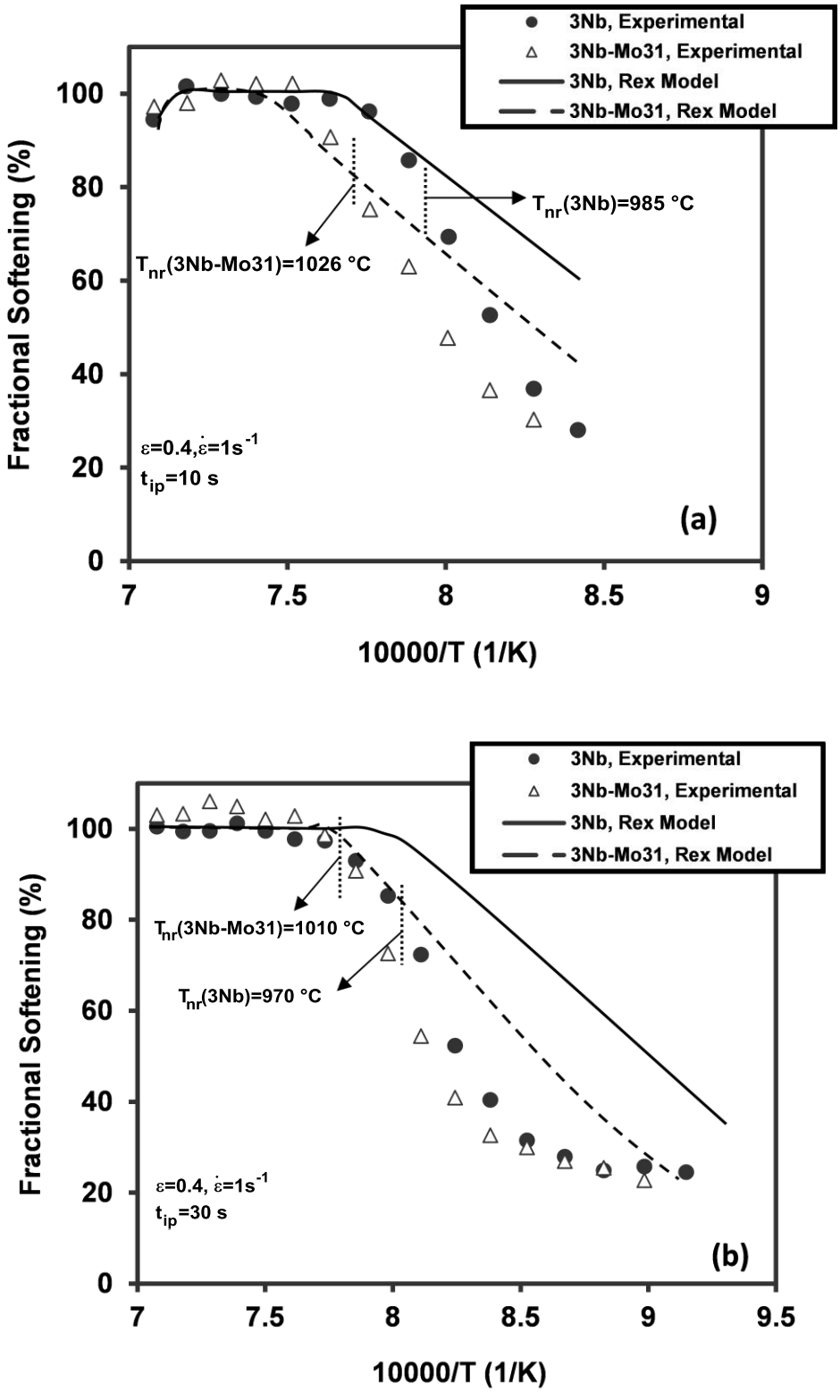

Figure 5. Experimental values and model predictions of fractional softening obtained with steels 3Nb and 3NbMo31 for ε = 0.4 and; (a) t_{ip} = 10 s and (b) t_{ip} = 30 s.

These results suggest that the differences reported in Figure 4, between the steels 3Nb and 3NbMo31 in the t_{ip} = 10 s and 30 s range of interpass times, were related to the additional solute drag effect of Mo. For t_{ip} = 5 s, the solute drag of Nb or Nb and Mo were the only retardation mechanisms active in both steels; however, for longer times strain induced precipitation interacts with recrystallization, and this was the mechanism responsible for the T_{nr} in the 3Nb steel (Figure 5).

In contrast, for the 3NbMo31 steel and in all the conditions tested, the non-recrystallization temperature was reached by a reduction in fractional softening due exclusively to solute drag; Nb(C,N) precipitation always occurred at temperatures well below the T_{nr}. This could also explain the decreasing trend observed in the T_{nr} values in Figure 4 for both 3NbMo16 and 3NbMo31 steels as the interpass time increases.

Phase Transformation

A complete characterization of phase transformations for the steels listed in Table I has been recently published [7]. Depending on the composition, the austenite conditioning and the cooling rate, a whole range of different microstructures are formed. When analyzing these complex microstructures, various classifications have been proposed to name them. In the present paper the ISIJ Bainite Committee notation is adopted, as the phases observed fit the proposed ones well. The phases are identified as Polygonal Ferrite (PF), Lamellar Pearlite (P), Degenerate Pearlite (DP), Quasipolygonal Ferrite (QF), Granular Ferrite (GF), Bainitic Ferrite (BF) and Martensite (M). Martensite–Austenite (M/A) constituents were also detected as secondary phases within QF and GF main phases. Figure 6 shows an example of the CCT diagrams obtained with the dilatometer and some characteristic microstructures for selected cooling rates for the 6NbMo31 steel. A combination of PF and DP was obtained for a slow cooling rate of 0.1 ºC/s, a mixture of QF and GF for the intermediate cooling rate of 5 ºC/s and, finally, M and BF were formed for the fastest cooling rate of 100 ºC/s.

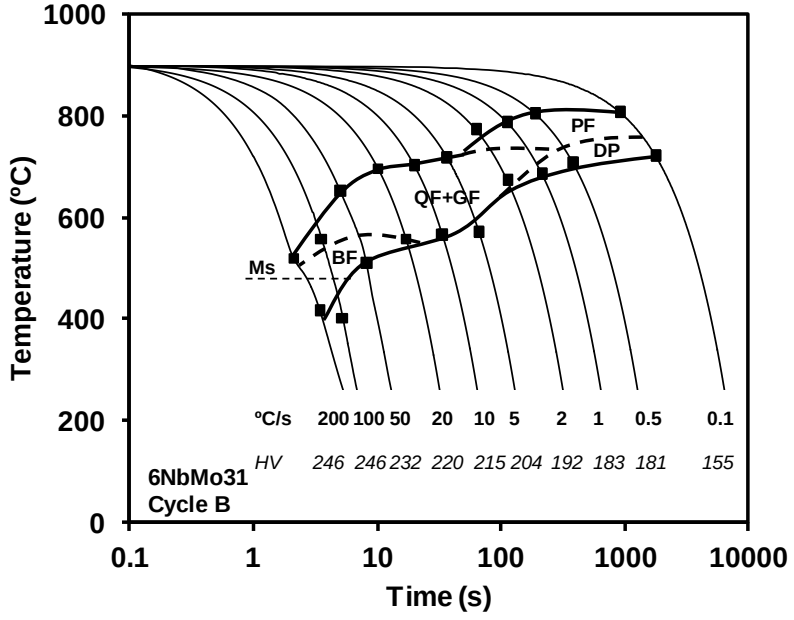

(a)

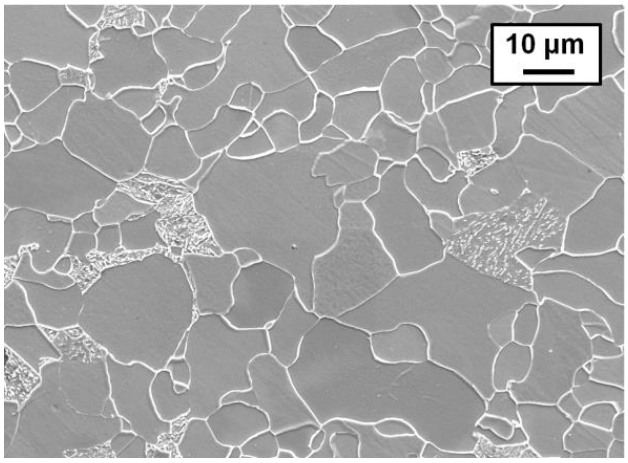

(b)

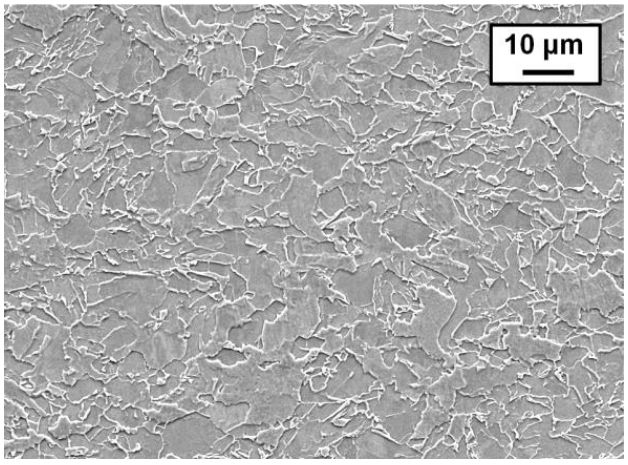

(c)

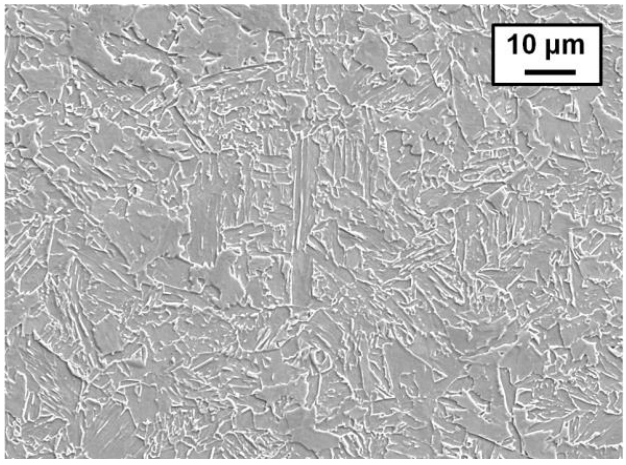

(d)

Figure 6. Examples of; (a) CCT diagram for steel 6NbMo31 transformed from deformed austenite (Cycle B) and several characteristic microstructures, (b) 0.1 ºC/s: PF+DP, (c) 5 ºC/s: QF+GF and (d) 100 ºC/s: M+BF.

Effect of Nb and Mo Additions

Figures 7 and 8, respectively, show the influence of Nb and Mo additions for phase transformations occurring from undeformed austenite (Cycle A). In Figure 7, the effect of Nb addition retarding PF formation is evident when the CMn and 3NbMo0 curves are compared. The Nb reduces the ferritic transformation field, as well as shifting the CCT diagram to lower bainitic transformation start temperatures (10-90 ºC) for the highest cooling rates. The effect of the increment of Nb from 0.03 to 0.06% on the transformation kinetics is negligible for the Nb steels transforming from undeformed austenite. Transformation start and finish temperatures remain similar both for ferritic and bainitic phases. This small effect of Nb in solution was also reported by Rees et al. [12]. In this case, it can be inferred that the retarding effect of a higher Nb level is counterbalanced by the smaller prior austenite grain size in steel 6NbMo0 [7].

The addition of Mo causes a decrease in the transformation start temperature when the 6NbMo0 and 6NbMo31 steels are compared (Figure 8), especially in the non-polygonal phase region (QF start temperature shifts down 0-40 ºC). For the steels containing a lower amount of Nb (Steels 3NbMo0 and 3NbMo31) a similar trend is observed. In this case, the PF start temperatures are decreased by 10-70 ºC and the QF start temperatures by 30-70 ºC. Therefore, the hardenability effect of Mo is confirmed for these compositions.

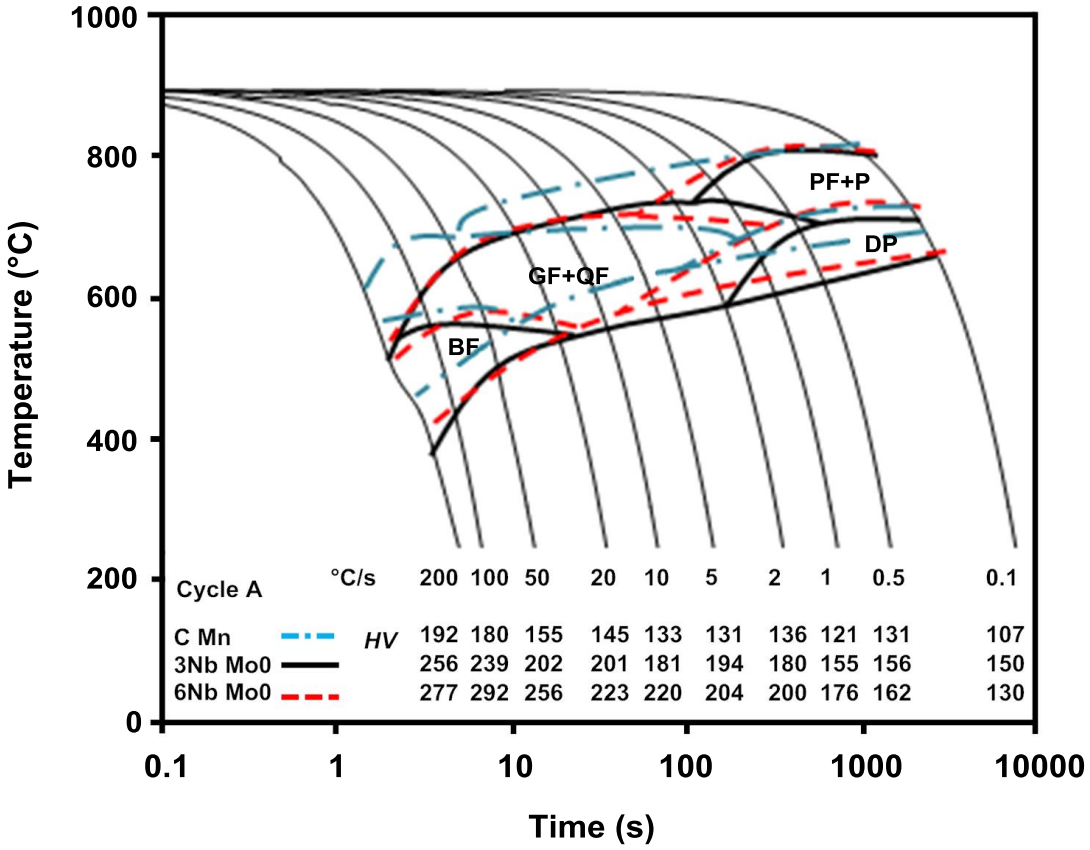

Figure 7. Effect of Nb on CCT diagrams obtained for Cycle A (undeformed austenite) - Steels CMn, 3NbMo0 and 6NbMo0.

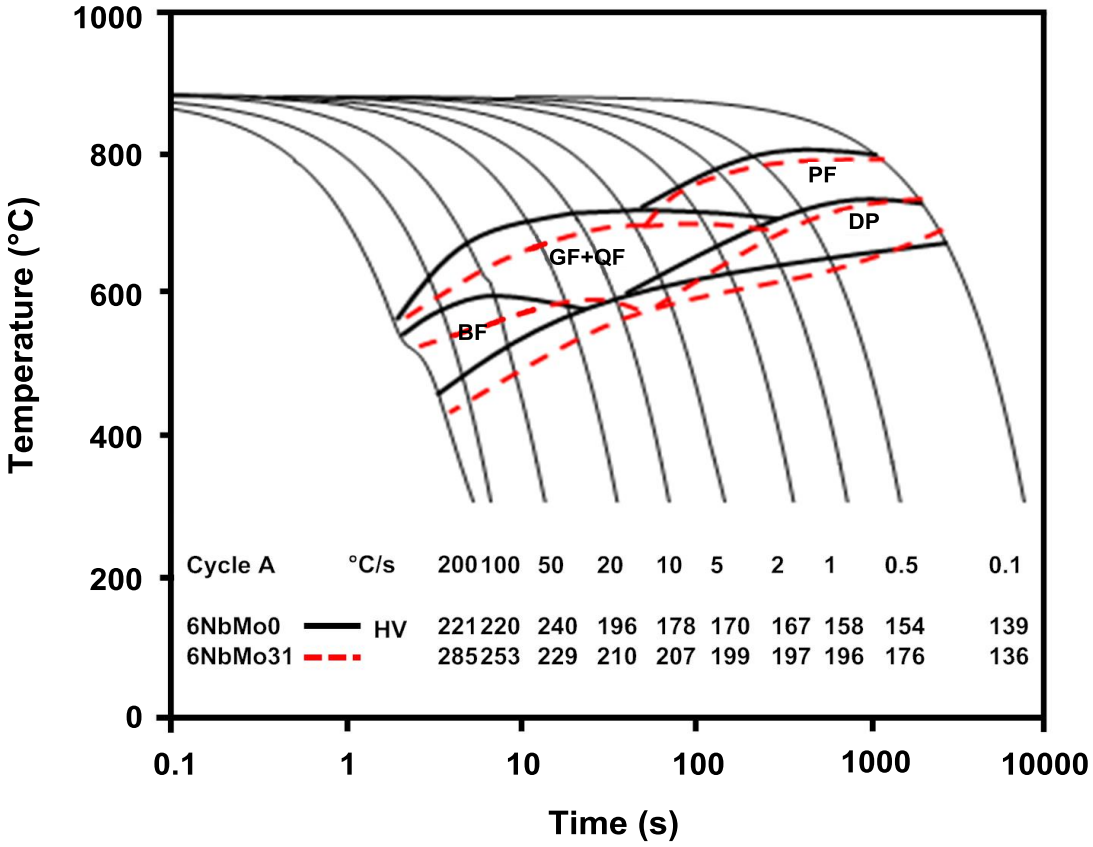

Figure 8. Effect of Mo on CCT diagrams obtained for Cycle A (undeformed austenite) - Steels 6NbMo0 and 6NbMo31.

Effect of the Amount of Deformation Retained in Austenite

The analysis of the effect of deformation on the CCT diagrams has been illustrated by comparing three diagrams for steel 6NbMo31 in Figure 9. Cycle A refers to transformation from undeformed austenite, Cycle B from austenite deformed to a strain of = 0.4 and Cycle C to a strain of 0.8 (see Figure 1). The deformation of the prior austenite promotes a slight acceleration of the transformations, this effect being more marked for the non-polygonal transformation start temperatures. The shift of the PF transformation field is important for Cycle C and the increment in the transformation start temperature as a result of accumulation of deformation in austenite is consistent with previously published data [13-15].

However, a limited effect of deformed austenite in low Nb steels was reported by Militzer et al. [16]. Similarly to what is observed in the present study, Lis et al. [17] and Olasolo et al. [18] observed that bainitic transformation was also accelerated in deformed austenite in the range of high cooling rates in 0.06%Nb microalloyed steels. These authors suggested that a higher dislocation density in the deformed austenite leads to a faster nucleation of the bainite laths.

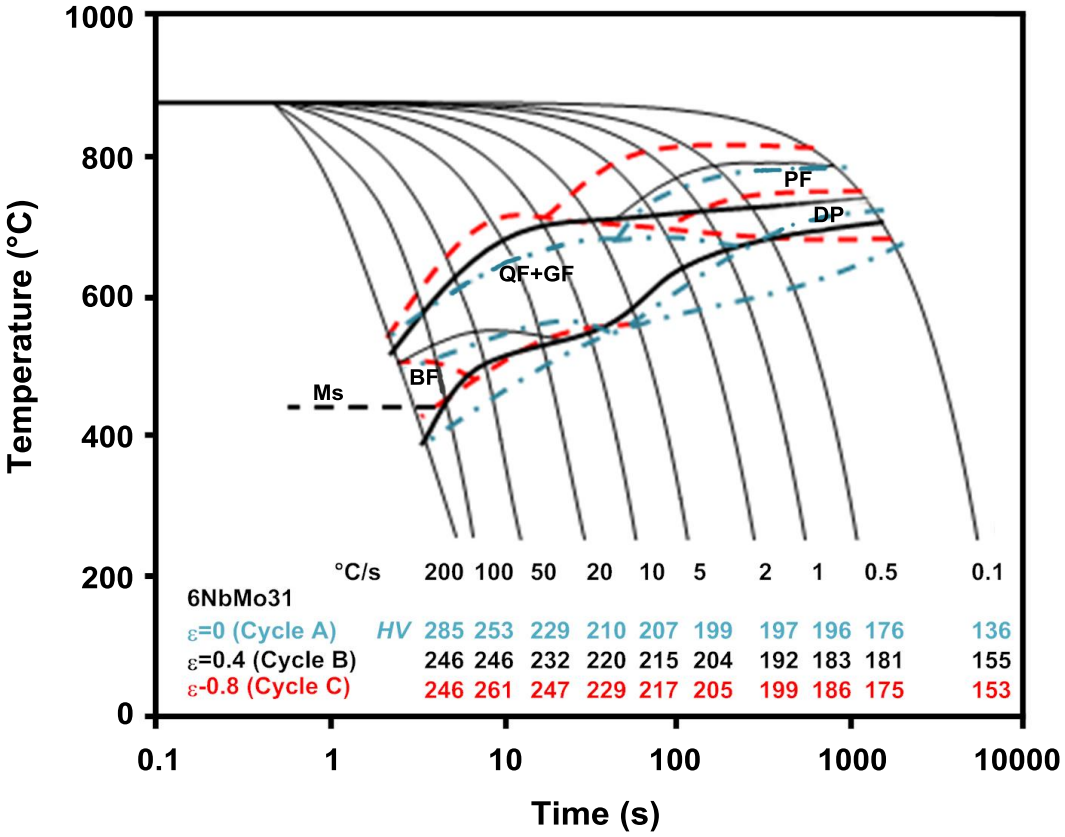

Figure 9. Comparison between the CCT diagrams obtained for steel 6NbMo31 in three austenite conditions (Cycle A: undeformed austenite, Cycle B: deformed austenite (ε = 0.4) and Cycle C: deformed austenite (ε = 0.8)).

Microstructural Unit Sizes and Homogeneity

CCT diagrams do not provide information regarding microstructural feature sizes. Therefore, a more detailed microstructural characterization is needed in order to evaluate the impact of composition on the mean unit sizes and homogeneity. Optical microscopy is suitable for ferritic microstructure characterization, however, when non-polygonal structures are measured, an EBSD analysis provides a more powerful tool to quantify them [19,20]. In order to quantify microstructure effect on strength and toughness, crystallographic unit sizes delimited by 4º and 15º misorientation low and high-angle boundaries were measured using the EBSD technique. Figure 10 exhibits the mean grain size as a function of the cooling rate for both misorientation criteria, for schedules B (ε=0.4) and C (ε=0.8) and different compositions. Figure 10(a) shows the influence of the cooling rate on the mean unit size taking the criterion of low angle misorientation of 4º into consideration for steels 6NbMo0 and 6NbMo31 and both schedules (Cycle B and Cycle C). As a general trend, the mean unit size decreases as the cooling rate increases. The refinement of the microstructure due to the cooling rate increasing is more noticeable in the ferritic range. On the other hand, a higher degree of deformation promotes a slight refinement at low cooling rates. This difference is more important if average values from

Cycle A are compared with those from Cycle B [7]. Finally, it was also observed that the addition of Mo leads to a slight refinement of the final microstructure.

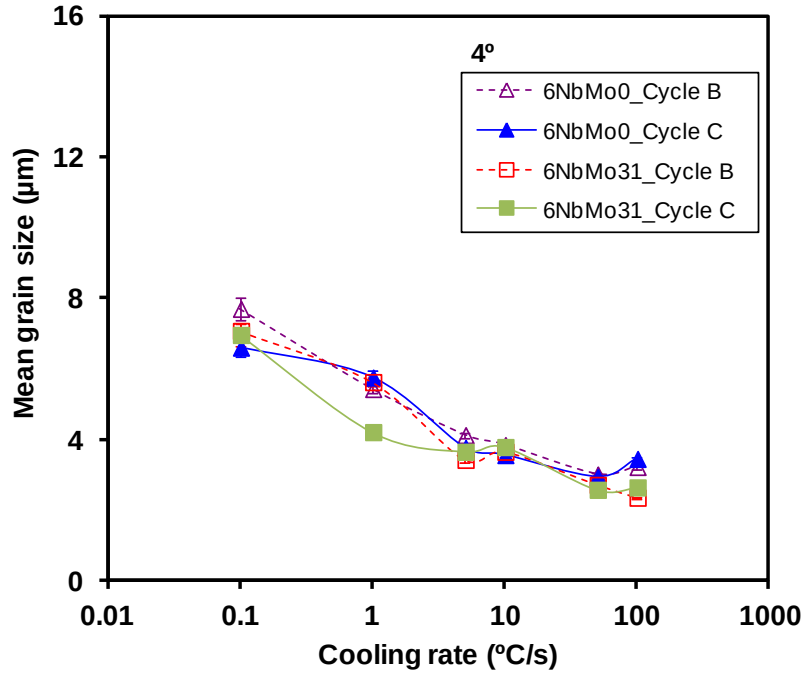

(a)

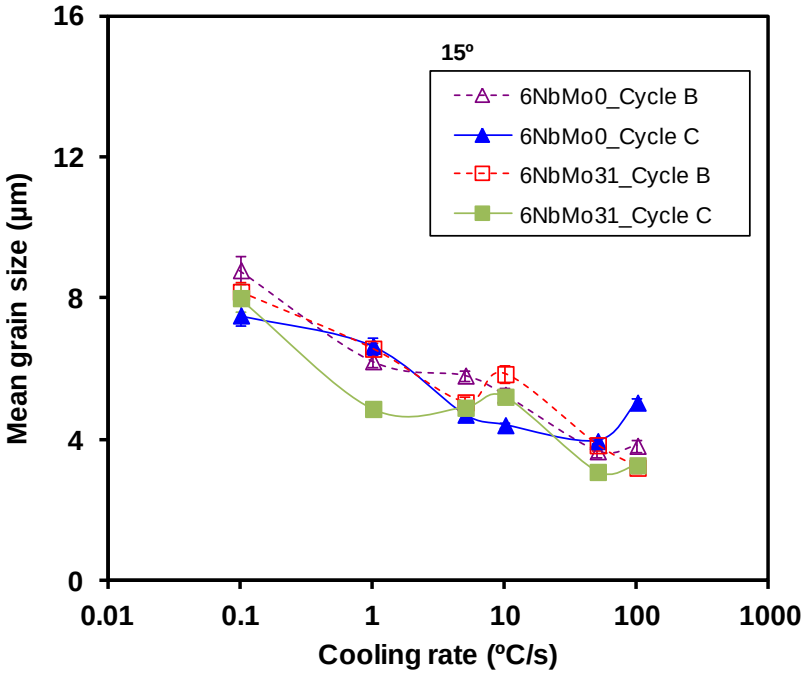

(b)

Figure 10. (a) Influence of cooling rate on the average unit size for steels 6NbMo0 and 6NbMo31 from both schedules, Cycle B (ε = 0.4) and Cycle C (ε = 0.8), using 4º threshold misorientation criterion and (b) using 15º threshold misorientation criterion.

When the 15º misorientation is used to define the unit size (see Figure 10(b)), unit sizes larger than for the 4º criterion are quantified in all conditions. Moreover, the mean grain size evolution as a function of the cooling rate is similar to the previously analyzed one with the 4º misorientation criterion. Even though there is not a significant influence of the accumulation of deformation for both compositions when the 4º criterion is used, the effect of a higher strain accumulation was more prominent when the high angle misorientation (15º) criterion is considered, especially in the bainitic range and for the Mo steel.

In order to evaluate the homogeneity of the resulting microstructure, the $Dc20\%/D_{mean}(15º)$ ratio as a function of the cooling rate has been plotted in Figure 11 for steels 6NbMo0 and 6NbMo31 and both schedules B and C. The Dc20% value refers to the cut-off grain size at 80% accumulated area fraction. Several trends can be observed on the $Dc20\%/D_{mean}(15º)$ ratio depending on the schedule and composition. For Cycle B, ferritic structures show the lowest values for the ratio and as QF and GF structures become dominant the ratio increases. This transition is reflected in a two-step regime and the ratio increases from approximately 2 to 7 for both steels. The behavior for Cycle C differs from that of Cycle B. In the 6NbMo0 steel, more homogeneous structures are observed when higher deformation is applied for the whole cooling rate range analyzed. However, for the highest cooling rates, the presence of BF promotes stronger heterogeneity in the 6NbMo31 steel and a later refinement when M is formed. This refinement was also observed for coarse austenite grain sizes [21]. Variant selection and nucleation inside grains is reported to be the most efficient way to reduce martensite/bainite block sizes and, consequently, to enhance homogeneity [22].

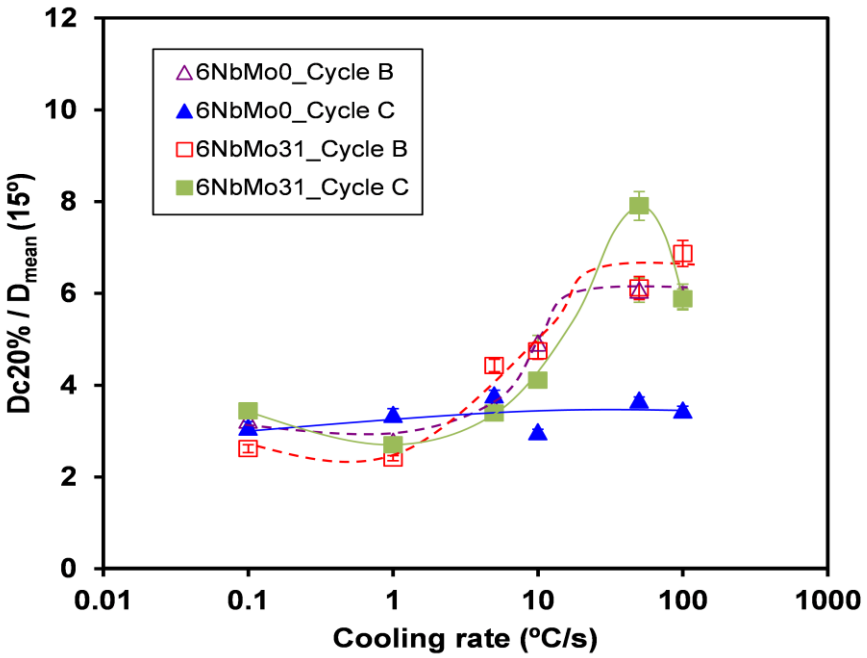

Figure 11. Evolution of $Dc20\%/D_{mean}(15º)$ ratio as a function of the cooling rate for steels 6NbMo0 and 6NbMo31 for both Cycles B ($\varepsilon = 0.4$) and C ($\varepsilon = 0.8$).

Microstructural Contributions to Mechanical Properties

The main goal of understanding the overall microstructural evolution during austenite hot working and final phase transformation is to acquire sufficient knowledge to link the mechanical properties of the steels with the resulting microstructure. So, several thermomechanical schedules have been carried out following the schemes shown in Figure 2. Tensile test samples were machined from the plane strain compression samples and a detailed microstructural characterization was performed.

Depending on the coiling temperature and the composition of the steel, the transformed microstructures change completely. Figure 12 exhibits several FEG-SEM micrographs for the steels containing the higher level of Nb at the coiling temperatures of 650 ºC, 550 ºC and 450 ºC (6NbMo0 in Figure 12(a), (b), (c) and 6NbMo31 in Figure 12(d), (e), (f)). In the steel 6NbMo0, for the higher coiling temperature of 650 ºC, a combination between PF and DP was obtained (see Figure 12(a)). By decreasing the coiling temperature, QF was formed accompanied by GF and the fraction of PF decreased considerably (see Figure 12(b)). Coiling at 450 ºC leads to the formation of a fully non-polygonal microstructure (QF and GF) (see Figure 12(c)). In the steel 6NbMo31, for the higher coiling temperatures (650 ºC and 550 ºC), M/A micro-regions retained between transformed phases were observed apart from the microstructures mentioned at those coiling temperatures (see Figure 12(d) and (e)). Furthermore, it is clearly evident that the amount of bainitic microstructure was higher when Mo was added. The microstructures related to the steels containing the low level of Nb (3NbMo0 and 3NbMo31) are similar to the previously analyzed microstructures.

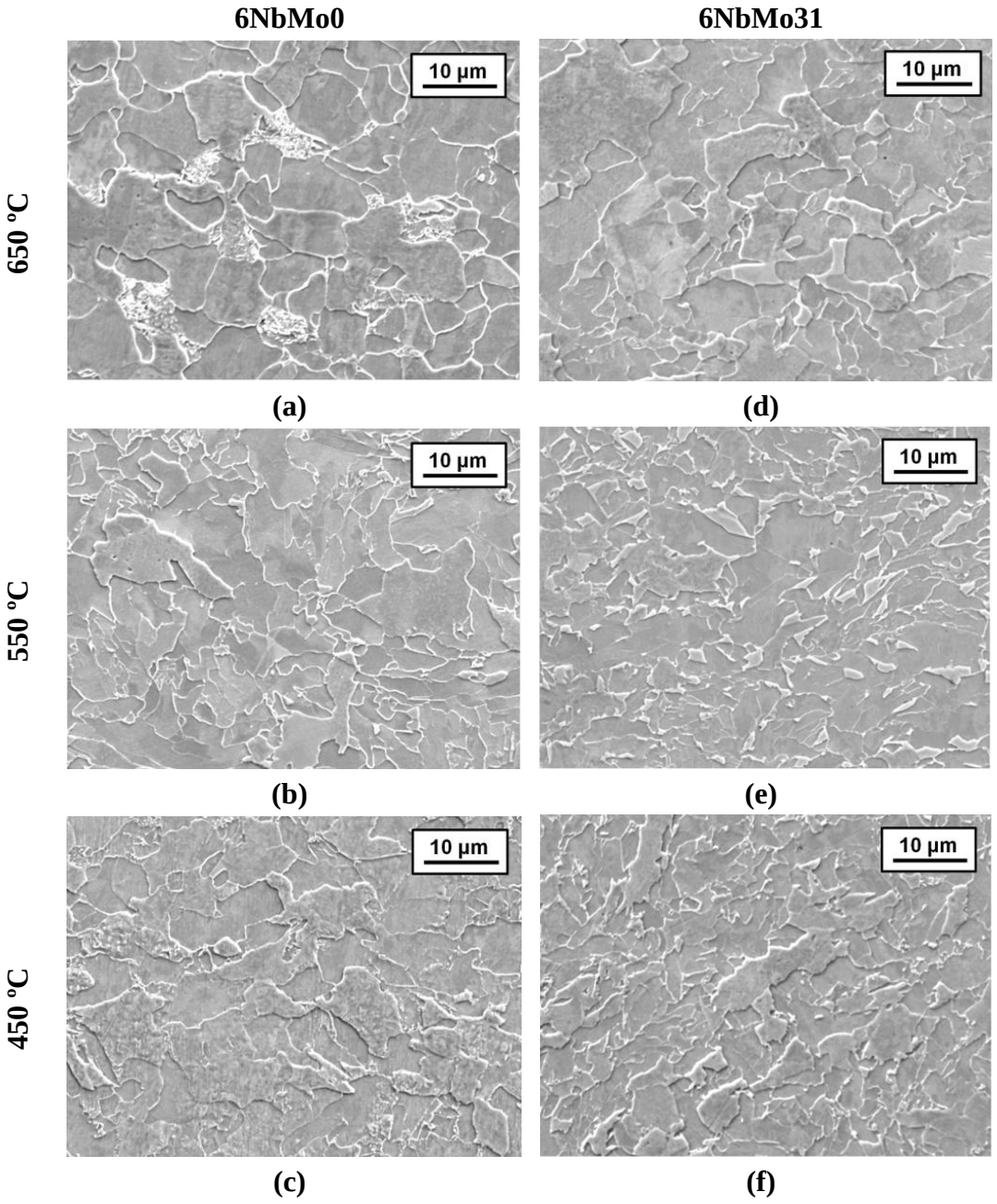

Figure 12. FEG-SEM micrographs of the steel 6NbMo0 and steel 6NbMo31 at different coiling temperatures; (a) and (d) 650 ºC, (b) and (e) 550 ºC and (c) and (f) 450 ºC.

Figures 13(a) and (b) exhibit tensile curves obtained for steel 3NbMo0 and steel 3NbMo31 at selected coiling temperatures (650, 550 and 450 ºC). The addition of Mo led to higher yield and tensile strengths, as well as lower elongation in all cases. Furthermore, for both compositions, higher yield and tensile strengths were obtained by decreasing the coiling temperature, with the exception of steel 3NbMo31 where the maximum strength is reached at the intermediate coiling temperature of 550 ºC.

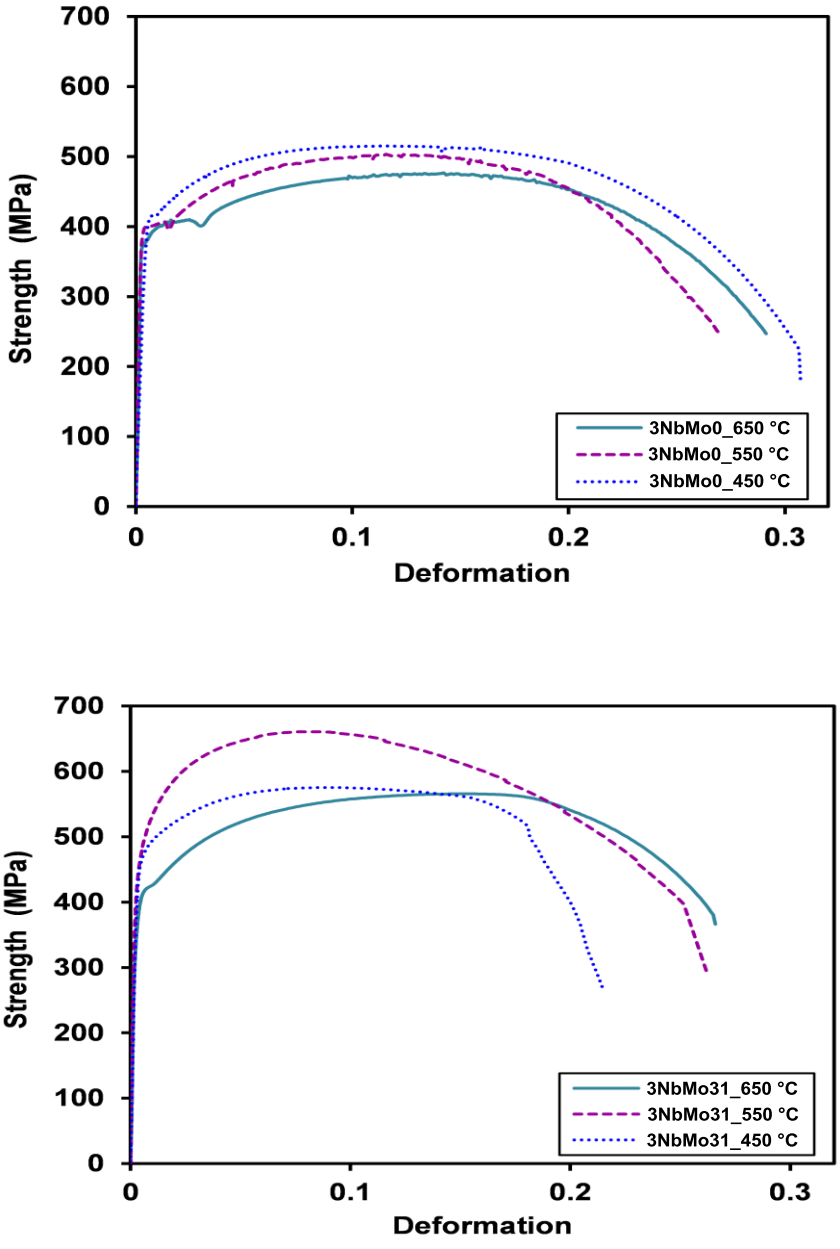

Figure 13. Engineering tensile curves obtained at different coiling temperatures (650, 550 and 450 ºC) for; (a) steel 3NbMo0 and (b) steel 3NbMo31.

In Table II, yield strength, tensile strength, elongation and area reduction values are shown for all the studied steels, for the entire range of coiling temperatures (650, 550 and 450 ºC). In reference to yield strength, YS values varied from 387 to 460 MPa, depending on the composition and applied coiling temperature. Higher YS values were obtained for Nb-Mo steels compared to the values obtained for steels containing Nb alone. Moreover, the highest YS value was obtained at the coiling temperature of 450 ºC in the steel 3NbMo31, reaching a value of 460 MPa. On the other hand, YS increased as coiling temperature decreased, due to a major presence of non-polygonal or bainitic microstructures (a mixture of QF and GF). Similar to what happened in YS values, significantly higher TS values were observed when Mo was added, reaching the highest tensile strength of 660 MPa at the intermediate coiling temperature (550 ºC) in the steel 3NbMo31.

Table II. Yield Strength (YS), Tensile Strength (TS), Elongation (%) and Area Reduction (%) Values for Different Compositions and Coiling Temperatures

Steel	Coiling T (ºC)	YS (MPa)	TS (MPa)	Elongation (%)	Area Reduction, RA (%)
3NbMo0	**650**	387	485	35	84
	550	401	506	36	85
	450	414	522	34	84
3NbMo31	**650**	393	571	28	77
	550	457	660	29	80
	450	460	575	34	89
6NbMo0	**650**	406	490	39	83
	550	410	512	39	86
	450	408	514	36	87
6NbMo31	**650**	426	594	33	71
	550	435	627	35	81
	450	473	582	33	82

Similar to what was found in the engineering tensile curves (Figure 13), a lower elongation was observed when Mo was added. Elongation is reduced from 39 to 33% at the coiling temperature of 650 ºC, for the steels 6NbMo0 and 6NbMo31 respectively. A significant influence of coiling temperature on the area reduction is observed, obtaining higher area reduction values as coiling temperatures decreases, except for steel 3NbMo0, where RA is approximately constant for the three coiling temperatures. Furthermore, as expected, the steels containing Mo exhibit lower area reduction values than those shown by the steels containing only Nb.

Strengthening Mechanisms

The yield strength (σ_y) of low carbon microalloyed steels can be expressed as a summation of different strengthening mechanisms [23]. Even though the lineal sum of components is the most widely used approach, other non-linear relationships have been also proposed so as to predict tensile properties. This is important when the contribution of different strengthening mechanisms is not equal and interactions between the different strengthening mechanisms exist. In this particular case, Equation 2, proposed by Yakubtsov et al. [24], shows the best fit between experimental and calculated values.

$$\sigma_y = ((\sigma_0 + \sigma_{ss} + \sigma_{ppt} + \sigma_{MA})^2 + \sigma_\rho{}^2 + \sigma_{gs}{}^2)^{0.5} \quad (2)$$

where σ_0 is the lattice friction stress, σ_{ss} is the solid solution strengthening, σ_{ppt} is the contribution of precipitation, σ_{MA} is the hardening due to the presence of MA islands, σ_ρ is the dislocation hardening and σ_{gs} is the strengthening effect of grain size. The equation shows a root mean summation and is suitable for combinations where the contributions of dislocations and grain size strengthening are relevant.

Strengthening Contribution due to Solid Solution. The contribution of solid solution to the yield strength was determined according to Equation 3 [25]. This equation has been widely used for low carbon steels.

$$\sigma_{ss} = \sigma_0 + 32.3Mn + 83.2Si + 11Mo + 354\ (N_{free})^{0.5} \quad (3)$$

where σ_0 is the lattice friction stress (σ_0=53.9 MPa) and the concentrations are expressed in weight percent. In the current study, the total amount of N is assumed to be precipitated in combination with Nb and consequently, there is no free N ($N_{free}=0$).

Strengthening Contribution Related to Grain Size. The contribution of the final microstructure grain size (σ_{gs}) follows the Hall-Petch relationship. Even though the Hall-Petch equation was developed for high angle boundaries, it has been progressively extended to subgrains and cell boundaries. The strengthening on account of sub-boundaries depends on their misorientation, resulting in a modified Hall-Petch exponent. In this work, a new approach recently published by Iza-Mendia et al. [26] has been adopted and the resulting equation is shown in Equation 4. The first term refers to low angle boundaries, while the second term is related to the contribution of high angle misorientation units. Therefore, especially in bainitic (QF+GF) microstructures, apart from high angle boundaries, it is important to take into account the contribution of boundaries in the interval 2<θ<15º, due to a high fraction of those kind of boundaries.

$$\sigma_{gs} = 1.05\alpha M\mu\sqrt{b}\left[\sum_{2\le\theta_i\le15^o} f_i\sqrt{\theta_i} + \sqrt{\frac{\pi}{10}}\sum_{\theta_i\ge15^o} f_i\right]\cdot d_{2^o}{}^{-\frac{1}{2}} \quad (4)$$

where α is a constant, M the average Taylor factor, μ is the shear modulus and b is the Burger's vector (α=0.3, M=3, μ=8x10^4 MPa and b=2.5 10^{-7} mm). θ_i and f_i, are the mean misorientation angle in the interval *i* and the relative frequency, respectively. d_{2^o} is the mean grain size considering a 2º criterion. These parameters are determined by EBSD.

In order to evaluate the interaction between the microstructural refinement and the contribution related to low angle boundary unit size, yield strength values are plotted in Figure 14 as a function of the mean unit size considering the low angle misorientation criteria of 2º. Two different trends are observed depending on whether the steel is microalloyed only with Nb or with both Nb and Mo. For Nb steels, there is not a clear dependence of yield strength on low angle boundary size. Nevertheless, for the Nb-Mo steels, where a very fine substructure is formed, with unit sizes ranging from 3 to 4 microns, a sharp increase in yield strength is measured as the unit size decreases.

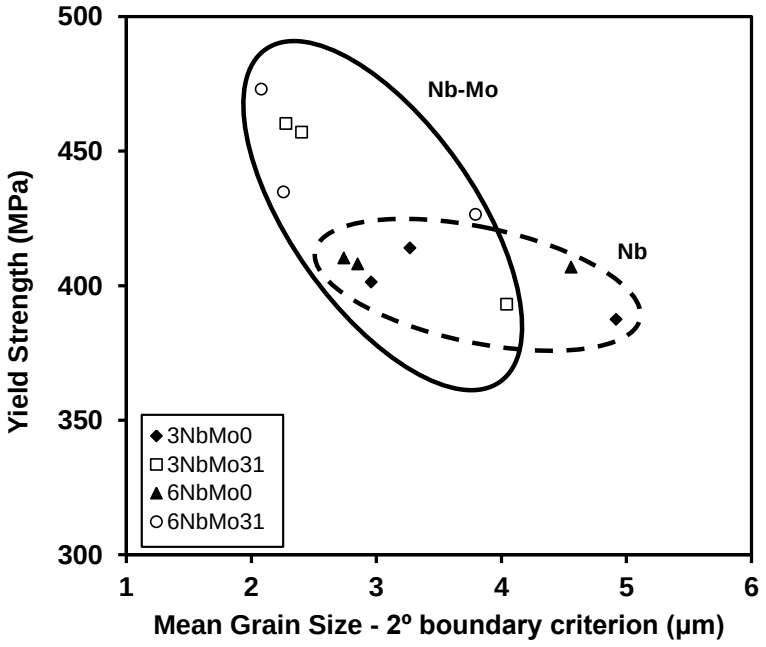

Figure 14. Yield strength as a function of 2º grain size for steels 3NbMo0, 3NbMo31, 6NbMo0 and 6NbMo31.

Strengthening Contribution due to Dislocations. In addition to solid solution and grain size contributions, the term related to dislocation density has to be considered. The contribution of the dislocation density can be expressed by Equation 5 [27].

$$\sigma_\rho = \alpha M \mu b \sqrt{\rho} \tag{5}$$

where α is a numerical factor, M is the Taylor factor, μ is the shear modulus, b is the Burger's vector and ρ is the dislocation density. A value of $\alpha M = 0.38$ has been established for body-centered cubic metals [28].

Strengthening due to dislocation density has been evaluated by other authors [26,27], through the analysis of the local misorientation gradients within a given region by means of the calculation of the Kernel Average Misorientation (KAM) parameter. In order to estimate dislocation density values from KAM data, Kubin and Mortensen's [29] approach was adopted:

$$\rho = \frac{2\vartheta}{ub} \tag{6}$$

where *u* is the unit length and *b* is the Burger's vector. The local misorientation value is achieved directly from EBSD data and is related to the kernel average misorientation value (ϑ). Kernel average misorientation for $\theta < 2^{o}$ and second neighbor criterion have been considered in order to evaluate the contribution of dislocation strengthening [27].

In Figure 15, calculated dislocation density values for the steels 3NbMo0, 3NbMo31, 6NbMo0 and 6NbMo31 are plotted as a function of coiling temperature. Dislocation density values vary from $3.42 \cdot 10^{14}$ to $5.92 \cdot 10^{14}$ m^{-2}, depending on the composition and applied coiling temperature. Even though in Nb steels the dislocation density remains nearly constant for all the range of coiling temperatures (ρ varies from $3.43 \cdot 10^{14}$ to $3.87 \cdot 10^{14}$ m^{-2}), when Mo is added a different trend is observed. Furthermore, the decreasing of coiling temperature (from 650 to 450 ºC) and consequently, the modification of the resultant microstructure from polygonal ferrite to a mixture of QF and GF, leads to a significant increment of dislocation density. For example, in steel 3NbMo31, ρ increases from $3.42 \cdot 10^{14}$ to $5.92 \cdot 10^{14}$ m^{-2}, when decreasing the coiling temperature from 650 to 450 ºC.

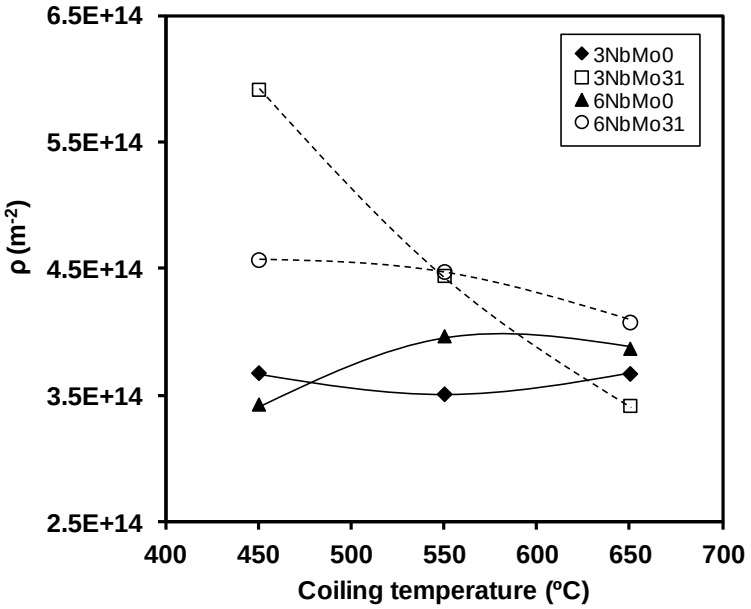

Figure 15. Dislocation density as a function of coiling temperature for all the steels studied (3NbMo0, 3NbMo31, 6NbMo0 and 6NbMo31).

Strengthening Contribution Caused by Precipitation. Precipitation strengthening has been successfully described by the Ashby-Orowan model (Equation 7) [30].

$$\sigma_{ppt} = 10.8 \frac{f_v^{0.5}}{x} \ln\left(\frac{x}{6.125 \cdot 10^{-4}}\right) \quad (7)$$

where f_v is the volume fraction of precipitates and x the mean planar intercept diameter of the particles (μm). Precipitate size distributions and average sizes, for each steel (3NbMo0, 3NbMo31, 6NbMo0 and 6NbMo31) and selected coiling temperatures (650, 550 and 450 ºC) were measured [31]. Finer precipitate mean sizes and higher fractions were measured in the Nb-Mo steels compared to Nb steels with the same level of Nb.

One of the biggest limitations for evaluating the contribution of precipitation hardening is to achieve an accurate calculation of the volume fraction of precipitates [32,33]. Even though the limitations of extraction replicas are widely known, an approximate volume fraction of precipitates was measured by means of TEM. The measurements of precipitate densities (amount of precipitates per unit area) of each steel and selected coiling temperatures (650, 550 and 450 ºC) were performed [31]. The estimation of the volume fraction of precipitates was achieved by means of Equation 8 [34].

$$f_V = k \frac{\pi}{6} N_S (x^2 + \sigma^2) \quad (8)$$

where k is a correction factor, N_s is the number of particles per unit area, x is the average particle size and σ is the standard deviation from x. A correction factor of 1/4 was applied based on a method that considers an estimated sampling depth for precipitates captured by replicas which is related to the approximate ratio between the average diameter of the small particles and the diameter of the largest particles captured by the replicas [33].

Strengthening Contribution Caused by M/A Islands. An additional strengthening effect limited to microstructures with the presence of M/A islands has to be taken into account. This contribution is proportional to the M/A volume fracion, f_{MA}, and was determined according to Equation 9 [35].

$$\sigma_{MA} = 900 f_{MA} \quad (9)$$

Evaluation of Strengthening Contributions

Taking into account all the individual strengthening contributions estimated according to the methodology described above, yield strength values were calculated for each composition and coiling temperature. These values are summarized in Table III and compared with the measured ones. Within the limitations of the method a satisfactory result is obtained in most cases. The biggest differences between calculated and measured values are achieved at the coiling temperature of 450 ºC. The precipitation strengthening contribution is expected to be underestimated in these cases. However, it can be concluded that the proposed strategy is useful for the interpretation of each particular contribution to the overall yield strength.

Table III. Comparison Between Experimental and Calculated Yield Strengths

	YIELD STRENGTH (MPa)							
$T_{coiling}$ (ºC)	**3NbMo0**		**3NbMo31**		**6NbMo0**		**6NbMo31**	
	σ_{y_calc}	**σ_{y_exp}**	**σ_{y_calc}**	**σ_{y_exp}**	**σ_{y_calc}**	**σ_{y_exp}**	**σ_{y_calc}**	**σ_{y_exp}**
650 ºC	341	388	374	393	349	407	392	426
550 ºC	387	401	429	457	415	410	475	435
450 ºC	373	414	412	460	414	408	422	473

The estimated individual strengthening contributions, considering Equation 2, are plotted in Figure 16. It is clearly evident that the grain size strengthening is the most relevant contribution, with relative percentages between 51% and 69%, depending on the composition and coiling temperature. The highest influence of the grain size refinement was obtained for steel 6NbMo31 at the lowest coiling temperature of 450 ºC. Regarding dislocation strengthening, higher strength values are obtained for lower coiling temperatures, especially in Nb-Mo steels, due to a major fraction of non-polygonal microstructures at low coiling temperatures. For example, in the steel 3NbMo31, the strengthening caused by dislocations increased from 13% to 19% by reducing the coiling temperature from 650 ºC to 450 ºC. Finally, Figure 16 exhibits a negligible effect of precipitation in steel 3NbMo0 (contribution from 3% to 7%). However, the influence of a fine precipitation is higher in the steels containing the higher level of Nb, due to a higher amount of solute Nb available for precipitation during transformation. In addition, Figure 16 shows that the highest contribution of precipitation was achieved at the intermediate coiling temperature (550 ºC) in the steel 6NbMo31.

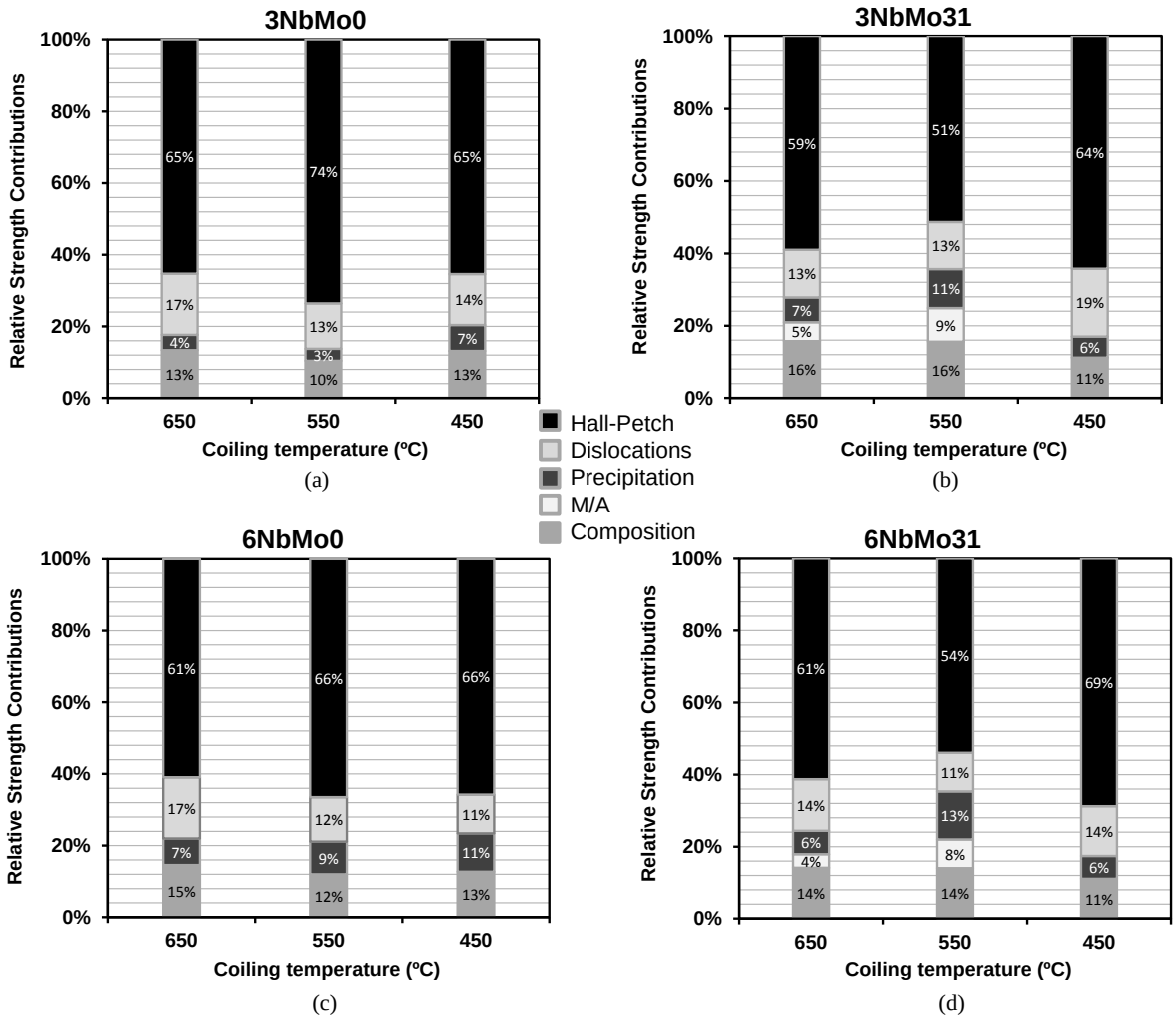

Figure 16. Strengthening contributions for steel 3NbMo0, 3NbMo31, 6NbMo0 and 6NbMo31.

Conclusions

Regarding austenite conditioning, Mo addition to Nb microalloyed steels results in a retardation of recrystallization kinetics due to the solute drag effect. However, this effect is weaker in the 0.06%Nb steels compared to the 0.03%Nb steels. A previous equation available for predicting the 50% recrystallization time, $t_{0.5}$, for Nb and Nb-Ti steels was extended to Nb-Mo steels, assuming an effective Nb level which captures the different solute drag contribution of Mo at the different Nb levels. The Nb and Mo solute drag effect seems to govern the non-recrystallization temperature, T_{nr}, in the Mo-Nb steels. Nevertheless, the addition of Mo to Nb microalloyed steels has other effects on the T_{nr} value, depending on the Nb content. In the range of medium Nb contents (0.03%Nb), the additional solute drag effect produced by Mo allows the T_{nr} values to be higher in the Nb-Mo than in the Nb steels. However, increasing the Nb content to values as high as 0.06%Nb, the acceleration of strain induced precipitation makes the contribution of Mo to solute drag, less relevant.

In terms of phase transformations, the addition of Mo to Nb steels ensures a higher retention of accumulated deformation before transformation. For low and intermediate cooling rates, the retained deformation favors the formation of polygonal phases, decreases the unit size of the phases formed and therefore, reduces the risk of the presence of heterogeneous structures.

An increase in the amount of accumulated strain provides an improvement in microstructural homogeneity; this improvement being more important for ferritic structures. Therefore, an optimized combination of chemical composition, thermomechanical schedule and cooling strategy in Nb-Mo microalloyed steels is needed in order to maximize the amount of applied strain below the non-recrystallization temperature, and consequently promote finer and more homogeneous structures.

Different strengthening mechanisms contribute to the high strength of microalloyed steel. The quantification of each strengthening contribution has shown that grain refinement plays a major role for the present steels, accounting for up to 60-70% of the yield strength. The addition of Mo to Nb microalloyed steels promotes the formation of a low angle misorientation substructure which enhances the strengthening effect arising from grain size reduction. The combination of Nb and Mo reduces the precipitate size and therefore, increases the strengthening contribution of fine carbides precipitated at low temperatures.

Acknowledgments

The financial support of the Spanish Ministry of Economy and Competitiveness (MAT2009-09250 and MAT2012-31056) and the Basque Government (PI2011-17) is gratefully acknowledged.

References

1. S.G. Jansto, "Niobium-bearing Steel Development for Value-added Structural Applications," *Proceedings of New Developments on Metallurgy and Applications of High Strength Steels Conference*, Buenos Aires, (2008), 1313.

2. D. Bhattacharya, *Proceedings of 6th International Conference on High Strength Low Alloy Steels, HSLA 2011*, Beijing, China, (2011), CD-Rom.

3. H. Mohrbacher, "Phase Transformation Study in Nb-Mo Microalloyed Steels Using Dilatometry and EBSD Quantification," *Proceedings of International Seminar on Applications of Mo in Steels,* Beijing, (2010), 75.

4. X. Sun and Q. Yong, "Phase Transformation Study in Nb-Mo Microalloyed Steels Using Dilatometry and EBSD Quantification," *Proceedings of International Seminar on Applications of Mo in Steels,* Beijing, (2010), 61.

5. O. Kwon and A.J. DeArdo, "Effect of Precipitation on the Recrystallization Behavior of a Nb Containing Steel," *Acta Metallurgica et Materialia*, 39 (1991), 529.

6. D.Q. Bai et al., "Effect of Deformation Parameters on the No-recrystallization Temperature in Nb-bearing Steels," *Metallurgical Transactions A,* 24 (10) (1993), 2151.

7. N. Isasti et al., "Phase Transformation Study in Nb-Mo Microalloyed Steels Using Dilatometry and EBSD Quantification," *Metallurgical and Materials Transactions A,* 44 (8) (2013), 3552 – 3563 (DOI: 10.1007/s11661-013-1738-3).

8. A.I. Fernández et al., "Static Recrystallization Behaviour of a Wide Range of Austenite Grain Sizes in Microalloyed Steels," *The Iron and Steel Institute of Japan International*, 40 (9) (2000), 893-901.

9. M.G. Akben and J.J. Jonas, "Influence of Multiple Microalloy Additions on the Flow Stress and Recrystallization Behavior of HSLA Steels," *HSLA Steels: Technology and Applications*, ed. M. Korchynsky (ASM, 1983), 149.

10. P. Uranga et al., "Modeling of Austenite Grain Size Distribution in Nb Microalloyed Steels Processed by Thin Slab Casting and Direct Rolling (TSRD) Route," *The Iron and Steel Institute of Japan International,* 44 (2004), 1416.

11. B. Pereda, B. López and J.M. Rodriguez-Ibabe, "Increasing the Non-Recrystallization Temperature of Nb Microalloyed Steels by Mo Addition", eds. A.J. DeArdo, C.I. Garcia, *Proceedings of the International Conference on Microalloyed Steels: Processing, Microstructure, Properties and Performance,* Pittsburgh, AIST, Warrendale, PA, (2007), 151-159.

12. G.I. Rees et al., "The Effect of Niobium in Solid Solution on the Transformation Kinetics of Bainite," *Materials, Science and Engineering A*, 194 (1995), 179.

13. D.N. Hanlon, J. Sietsma and S. van der Zwaag, "The Effect of Plastic Deformation of Austenite on the Kinetics of Subsequent Ferrite Formation," *The Iron and Steel Institute of Japan International*, 41 (2001), 1028.

14. C. Calvo et al., "Influence of the Chemical Composition on Transformation Behaviour of Low Carbon Microalloyed Steels," *Materials, Science and Engineering A,* 520 (2009), 90.

15. R.Y. Zhang and J.D. Boyd, "Bainite Transformation in Deformed Austenite," *Metallurgical and Materials Transactions*, 41A (2010), 1448.

16. M. Militzer, E.B. Hawbolt and T.R. Meadowcroft, "Microstructural Model for Hot Strip Rolling of High Strength Low-alloy Steels," *Metallurgical and Materials Transactions*, 31A (2000), 1247.

17. A.K. Lis and J. Lis, "Effect of Hot Deformation and Cooling Rate on Phase Transformations in Low Carbon HN5MVNb Bainitic Steel," (Thermec 2006), *Materials Science Forum,* 539-543 (2007), 4620.

18. M. Olasolo et al., "Effect of Austenite Microstructure and Cooling Rate on Transformation Characteristics in a Low Carbon Nb–V Microalloyed Steel," *Materials, Science and Engineering A*, 528 (2011), 2559.

19. F. Gerdemann, et al, "Metallographic Characterization of Bainitic Microstructures," *International Conference on New Developments in Advanced High-Strength Sheet Steels*: *June 15-18, 2008 Orlando, Florida, U.S.A.* (Warrendale, PA: AIST, 2008) S. 93.

20. A.W. Wilson and G. Spanos, "Application of Orientation Imaging Microscopy to Study Phase Transformations in Steels," *Materials Characterization*, 46 (2001), 407.

21. N. Isasti et al., "Effect of Composition and Deformation on Coarse-grained Austenite Transformation in Nb-Mo Microalloyed Steels," *Metallurgical and Materials Transactions* 42A (2011), 3729.

22. T. Furuhara, N. Takayama and G. Miyamoto, "Key Factors in Grain Refinement of Martensite and Bainite," *Materials Science Forum*, 638-642 (2010), 3044.

23. F.B. Pickering, *Physical Metallurgy and the Design of Steels* (London, UK: Applied Science Publishers Ltd, 1978), 10.

24. I.A. Yakubtsov et al., "Strengthening Mechanism in Dual-phase Acicular Ferrite + M/A Microstructures," *Proceedings of 42nd Mechanical Working and Steel Processing Conference,* Toronto, Ontario, (2000), 429.

25. F.B. Pickering and T. Gladman, "Metallurgical Developments in Carbon Steels, Iron and Steel Institute" (Special Report No. 81, London, 1963).

26. A. Iza-Mendia and I. Gutiérrez, "Generalization of the Existing Relations Between Microstructure and Yield Stress from Ferrite–Pearlite to High Strength Steels," *Materials, Science and Engineering A*, 561 (2013), 40.

27. M. Calcagnotto et al., "Orientation Gradients and Geometrically Necessary Dislocations in Ultrafine Grained Dual-phase Steels Studied by 2D and 3D EBSD," *Materials, Science and Engineering A*, 527 (2010), 2738.

28. A.S. Keh and S. Weissmann, "Deformation Substructure in Body-centered Cubic Metals," *Electron Microscopy and the Strength of Crystals*, eds. G. Thomas and J. Washburn, (New York, NY: Interscience, 1963), 231.

29. L.P. Kubin and A. Mortensen, "Geometrically Necessary Dislocations and Strain-gradient Plasticity: A Few Critical Issues," *Scripta Materilia*, 48 (2003), 119.

30. T. Gladman, "Precipitation Hardening in Metals," *Materials Science and Technology*, 15 (1999), 30.

31. N. Isasti, “Estudio de las Transformaciones de Fase en Aceros Microaleados con Nb y Nb-Mo. Relación Entre Microestructura y Propiedades Mecánicas” (Ph.D. thesis, San Sebastian, University of Navarra, 2013).

32. J. Lu, D. Ivey and H. Henein, “A Review of Methods to Quantify Nanoscale Precipitates in Microalloyed Steels - Part I,” *AIST Transactions*, 10 (2013), 232.

33. K. Poorhaydari and D.G. Ivey, “Precipitate Volume Fraction Estimation in High Strength Microalloyed Steels,” *Canadian Metallurgical Quarterly*, 48 (2009), 115.

34. M.F. Ashby and R. Ebeling, “On the Determination of the Number, Size, Spacing and Volume Fraction of Spherical Second-phase Particles from Extraction Replicas,” *Transactions of the Metallurgical Society of AIME,* 236 (1966), 1396.

35. M.E. Bush and P.M. Kelly, “Strengthening Mechanisms in Bainitic Steels,” *Acta Metallurgica*, 19 (1971), 1363.